

## Research Article

# Three-Dimensional Coprime Array for Massive MIMO: Array Configuration Design and 2D DOA Estimation

Pan Gong , Tanveer Ahmed , and Jianfeng Li 

College of Electronic and Information Engineering, Nanjing University of Aeronautics and Astronautics, Nanjing 211106, China

Correspondence should be addressed to Pan Gong; gongpan@nuaa.edu.cn

Received 25 July 2019; Revised 14 October 2019; Accepted 28 December 2019; Published 13 January 2020

Guest Editor: Raed A. Abd-Alhameed

Copyright © 2020 Pan Gong et al. This is an open access article distributed under the Creative Commons Attribution License, which permits unrestricted use, distribution, and reproduction in any medium, provided the original work is properly cited.

In massive multiple-input multiple-output (MIMO) systems, it is critical to obtain the accurate direction of arrival (DOA) estimation. Conventional three-dimensional array mainly focuses on the uniform array. Due to the dense arrangement of the sensors, the array aperture is limited and severe mutual coupling effects arise. In this paper, a coprime cubic array (CCA) configuration design is presented, which is composed of two uniform cubic subarrays and can extend the interelement spacing with a selection of three pairs of coprime integers. Compared with uniform cubic array (UCA), CCA achieves the larger array aperture and less MC effects. And the analytical expression of Cramer–Rao Bound (CRB) for CCA is derived which verifies that the proposed CCA geometry outperforms the conventional UCA in two-dimensional (2D) DOA estimation performance in massive MIMO systems. Meanwhile, we propose a computationally efficient 2D DOA estimation algorithm with high accuracy for CCA. Specifically, we utilize array mapping to extract two uniform arrays from the nonuniform array by exploiting the relation derived from the signal subspace and the two directional matrices. Then, we operate a reduced dimension process on the uniform arrays and convert the 2D spectrum peak searching (SPS) problem into one-dimensional (1D) one, which significantly reduces the computational complexity. In addition, we employ the polynomial root finding technique with a lower complexity instead of 1D SPS to further relieve the computational complexity. Simultaneously, with coprime property, the phase ambiguity problem is solved, which results from the large interelement spacing. Numerical simulation results demonstrate that the proposed algorithm is very computationally efficient without degradation of DOA estimation performance.

## 1. Introduction

Nowadays, massive multiple-input multiple-output (MIMO), known as large-scale MIMO, is considered as one of the promising technologies in the development of future wireless communication systems. Massive MIMO attracts considerable attention due to the high throughput, enhanced link reliability, and improved spectral efficiency [1, 2]. Also, massive MIMO can effectively reduce the latency and robustness to interference [3, 4], which are important factors in wireless communication systems.

Direction of arrival (DOA) estimation plays an important role in massive MIMO, since precise DOA estimation is vital for the base station (BS) to conduct downlink precoding or beamforming [5]. DOA estimation is also widely utilized in engineering applications, like radar, sonar, wireless

communication, and navigation [6–9]. Many classic DOA estimation algorithms [10–13] and plenty of derived algorithms [14–16] have been proposed to solve the DOA estimation problem. Most of these existing algorithms mainly utilize the conventional uniform array configurations [17, 18] with the interelement spacing no larger than typical half-wavelength to tackle the problem of phase ambiguity [19]. However, in the massive MIMO systems, with a large number of antennas, severe mutual coupling (MC) effects arise, which significantly affect the DOA estimation accuracy.

In recent years, a new configuration called coprime array [20] has been a hot research direction and attracts much attention since it can significantly enhance the degree of freedom (DOF) [21], improve the resolution [22], and relieve MC effects [23]. This motivates many studies of DOA

estimation using coprime array over the decade. In [24], a total angular search based algorithm by employing the multiple signals classification (MUSIC) algorithm was proposed. By exploiting the coprime property, the phase ambiguity problem is tackled. In [25], an ambiguity-free DOA estimation algorithm was proposed, which exploits the total information including self-information and mutual information to eliminate the ambiguity problem with high accuracy of DOA estimates. However, due to the total angular search, this algorithm results in large computational complexity. To deal with this obstacle, a partial spectral search (PSS) algorithm was introduced which only performs spectrum searching in a restricted sector and hence lowers the computational cost but has no effect on DOA estimation performance [26]. In the case of multiple sources, this algorithm will cause the target matching error when eliminating the phase ambiguity. To tackle the problem, an improved DOA estimation algorithm based on root-MUSIC was proposed in [27] for coprime linear array (CLA), which employs the relation between steering matrices and signal subspaces of two subarrays to achieve DOA estimation.

The algorithms mentioned above [24–27] were presented for one-dimensional (1D) DOA estimation, whereas, practically, two-dimensional (2D) DOA estimation possesses more importance, and various studies have been introduced [28–30]. In [28], the PSS algorithm for coprime planar array (CPA) was presented, which can reduce the computational complexity. A reduced dimension notion to achieve 2D DOA estimation was proposed in [29]. A generalized CPA geometry with more flexible array layouts was constructed for 2D DOA estimation [30], which can attain more DOFs compared with CPA configuration. However, spectrum peak searching (SPS) is involved in these mentioned works [28–30] and hence causes expensive computational cost.

In this paper, on the basis of the 1D CLA and 2D CPA, we construct a three-dimensional (3D) array geometry called coprime cubic array (CCA). In the context of massive MIMO systems [31, 32], MC effects become important which have a vital influence on DOA estimation accuracy. The geometry of CCA possesses the extended array aperture and can effectively reduce MC effects. Especially, in the cases with small elevations, the CCA obtains superior DOA estimation performance. Simultaneously, the Cramer–Rao Bound (CRB) is derived which demonstrates that the proposed CCA geometry outperforms the conventional uniform cubic array (UCA) configuration [33–35]. In addition, we propose an array mapping and reduced dimension based on computationally efficient MUSIC (AMRD-MUSIC) algorithm to estimate 2D DOAs. Different from the conventional multiple-dimensional MUSIC (MD-MUSIC) algorithm, where 2D SPS involves a tremendous computation burden, in the proposed algorithm, we utilize array mapping to extract two uniform arrays from the nonuniform array by exploiting the relation derived from the signal subspace and the two directional matrices. Then, we operate a reduced dimension process on the uniform arrays and convert the 2D spectrum peak searching (SPS) problem into 1D one, which significantly reduces the computational

complexity. In addition, we employ the polynomial root finding technique with a lower complexity instead of 1D SPS to further reduce the computational complexity. Meanwhile, according to the coprime property, the phase ambiguity problem is solved which results from large interelement spacing and the proposed algorithm obtains paired angles automatically. Numerical simulation results demonstrate that the proposed AMRD-MUSIC algorithm can significantly reduce the computational complexity cost with no degradation of DOA estimation performance.

Specifically, we summarize the main contributions of this paper.

- (1) In massive MIMO systems, conventional 3D array mainly focuses on the uniform array, which limits the array aperture and suffers from severe MC effects due to the dense location of sensors. We construct a CCA configuration which can achieve the larger array aperture and less MC effects compared with UCA. In addition, the analytical expression of CRB with CCA is derived and simulations demonstrate that the proposed CCA performs better DOA estimation performance than the conventional UCA configuration.
- (2) We propose an AMRD-MUSIC algorithm for 2D DOA estimation that can achieve almost the same DOA estimation performance as classic MD-MUSIC algorithm but with lower computational complexity. Through array mapping, we extract two uniform arrays from the nonuniform array and operate a reduced dimension on these two arrays to reduce 2D SPS into 1D one, which can effectively lower the computational complexity. To further reduce complexity, we utilize the polynomial root finding technique with a lower complexity instead of SPS. Therefore, computational complexity obtains a significant decrease.
- (3) The proposed algorithm can achieve the full DOFs and obtain DOA estimates with pairing automatically.

Section 2 introduces the array configuration and signal model. In Section 3 and Section 4, we present the proposed algorithm and analyse the performance of the proposed algorithm, respectively. Sections 5 and 6 provide numerical simulations and conclusions, respectively.

*Notations* 1. We use  $(\cdot)^T$  as the transpose, and  $(\cdot)^H$  is utilized as the conjugate transpose.  $\odot$  signifies *Khatri–Rao* product and  $\otimes$  denotes *Kronecker* product.  $E(\cdot)$  is expectation.  $D_m(\cdot)$  is a diagonal matrix that is formed of the  $m$ -th row of the matrix.  $\text{angle}(\cdot)$  is a phase operator.

## 2. Array Configurations and Signal Model

*2.1. Uniform Cubic Array.* UCA geometry is designed with  $M \times N \times J$  sensors, where  $M$  denotes the number of sensors in the  $x$ -axis,  $N$  and  $J$  denote the number of sensors in the  $y$ -axis and  $z$ -axis, respectively. The interelement spacing of UCA is  $d_x = d_y = d_z = \lambda/2$ , which denotes the interelement

spacing of  $x$ -axis,  $y$ -axis, and  $z$ -axis, respectively.  $\lambda$  is wavelength. Figure 1(a) shows an example of UCA with  $M = N = J = 3$ .

**2.2. Coprime Cubic Array.** For UCA configuration, the array aperture is limited by the interelement spacing no larger than conventional half-wavelength. Simultaneously, MC effects exist due to the dense location of sensors. Based on CLA and CPA, we propose a CCA configuration, which can effectively increase the array aperture and decrease the MC effects.

**Definition 1** (coprime cubic array (CCA)). The CCA consists of two subarrays. The first subarray is composed of  $M_1 \times N_1 \times J_1$  sensors with the interelement spacing of  $d_{x1} = M_2\lambda/2$  in  $x$ -axis direction,  $d_{y1} = N_2\lambda/2$  in  $y$ -axis direction, and  $d_{z1} = J_2\lambda/2$  in  $z$ -axis direction. For the second subarray, it contains  $M_2 \times N_2 \times J_2$  elements and  $d_{x2} = M_1\lambda/2$ ,  $d_{y2} = N_1\lambda/2$ ,  $d_{z2} = J_1\lambda/2$ , where  $M_1, M_2, N_1, N_2$  and  $J_1, J_2$  are coprime integer pairs and stand for the number of sensors in  $x$ -axis,  $y$ -axis, and  $z$ -axis, respectively. Therefore, there are  $T_{CCA} = M_1N_1J_1 + M_2N_2J_2 - 1$  sensors in total. Figure 1(b) is an example of CCA geometry with  $M_1 = 3, N_1 = 2, J_1 = 3$  and  $M_2 = 2, N_2 = 3, J_2 = 2$ .

In the following part, we compare the array performance in array aperture and MC effects of UCA and CCA, respectively.

**2.3. Array Aperture Comparison.** In this subsection, we compare the array aperture of UCA and CCA in the same cases. For a fair comparison, we assume that the number of sensors in UCA and CCA is basically the same. According to [36], we can compute the array apertures of these arrays, which are denoted as  $\Gamma_{UCA}$  and  $\Gamma_{CCA}$ :

$$\Gamma_{UCA} = (M-1)(N-1)(J-1) \times \frac{\lambda^3}{8},$$

$$\Gamma_{CCA} = \max\left( (M_1-1)M_2(N_1-1)N_2(J_1-1)J_2 \frac{\lambda^3}{8}, \right. \\ \left. (M_2-1)M_1(N_2-1)N_1(J_2-1)J_1 \frac{\lambda^3}{8} \right). \quad (1)$$

For example, we set the UCA with  $M = 4, N = 4, J = 6$ , so the total number of sensors in UCA is  $T_{UCA} = M \times N \times J = 4 \times 4 \times 6 = 96$ . One subarray of CCA is of  $M_1 = 5, N_1 = 2, J_1 = 3$  and the other subarray is of  $M_2 = 4, N_2 = 3, J_2 = 5$ . The number of sensors in CCA is  $T_{CCA} = M_1 \times N_1 \times J_1 + M_2 \times N_2 \times J_2 - 1 = 89$  in total. We can note that the CCA has fewer number of sensors than UCA. As a result, for the two given arrays, the array aperture can be obtained as  $\Gamma_{UCA} = 5.625\lambda^3, \Gamma_{CCA} = 90\lambda^3$ . So we have

$$\Gamma_{UCA} < \Gamma_{CCA}. \quad (2)$$

It can be seen that the proposed CCA configuration can effectively enlarge the array aperture with fewer sensors.

**2.4. Mutual Coupling Effects Comparison.** Array signal models usually neglect the MC between the sensors. In practical application, the MC effects between the closely located sensors should be considered. Without loss of generality, we employ a coupling matrix  $\mathbf{C} \in \mathbb{C}^{T \times T}$ , where  $T$  denotes the total number of sensors in the array. In general, the expression of  $\mathbf{C}$  is very complicated. According to [37], for given UCA and CCA configurations,  $\mathbf{C}$  can be denoted approximately by a B-banded Toeplitz matrix as follows:

$$\mathbf{C}_{i,j} = \begin{cases} c_{|d_i-d_j|}, & |d_i-d_j| \leq B, \\ 0, & |d_i-d_j| > B, \end{cases} \quad (3)$$

where the value of  $\mathbf{C}_{i,j}$  is inversely proportional to sensor distance and satisfies  $1 = c_0 > |c_1| > |c_2| > \dots > |c_B| > |c_{B+1}| = 0$ .  $B$  is a constant and  $d_i$  denotes the positions of sensors.

According to [37], the coupling leakage can be exploited to evaluate the total MC

$$L = \frac{\|\mathbf{C} - \text{diag}(\mathbf{C})\|_F}{\|\mathbf{C}\|_F}, \quad (4)$$

where  $\|\mathbf{C} - \text{diag}(\mathbf{C})\|_F$  is the amount of MC. It is indicated that the smaller  $L$  is, the less MC is.

We compare the coupling leakages of the given UCA of  $M = 4, N = 4, J = 6$  and CCA of  $M_1 = 5, N_1 = 2, J_1 = 3$  and  $M_2 = 4, N_2 = 3, J_2 = 5$ . The total number of sensors of UCA and CCA is  $T_{UCA} = M \times N \times J = 4 \times 4 \times 6 = 96$  and  $T_{CCA} = M_1 \times N_1 \times J_1 + M_2 \times N_2 \times J_2 - 1 = 89$ , respectively. Hence, we have  $\mathbf{C}_{UCA} \in \mathbb{C}^{96 \times 96}$  and  $\mathbf{C}_{CCA} \in \mathbb{C}^{89 \times 89}$ . So the coupling coefficients can be computed by the following:

$$c_d = \begin{cases} 1, & d = 0, \\ 0.3e^{j\pi/3} \cdot \frac{e^{-j(d-1)\pi/8}}{d}, & 1 \leq d \leq B, \\ 0, & d > B, \end{cases} \quad (5)$$

where  $B = 3$  and  $d$  denotes the distance between the random two sensors. Then, we compute the coupling leakages of UCA and CCA as  $L(T_{UCA}) = 0.7588$  and  $L(T_{CCA}) = 0.2829$ , respectively. It can see that the proposed CCA can effectively decrease the MC effects.

$$L_{CCA} < L_{UCA}. \quad (6)$$

Table 1 shows the comparison of array aperture and coupling leakage for UCA and CCA in the same conditions. From Table 1, we can see that the proposed CCA configuration has the least sensors but outperforms the UCA in array aperture and MC effects. In addition, the CCA achieves better DOA estimation performance that is shown in Section 5. Therefore, in the following part, we employ the CCA into consideration.

**2.5. Signal Model.** Assume that there are  $K$  far-field uncorrelated narrowband incident signals impinging on the CCA from  $\{(\theta_k, \phi_k) \mid \theta_k \in (0^\circ, 90^\circ), \phi_k \in (0^\circ, 180^\circ)\}$ ,

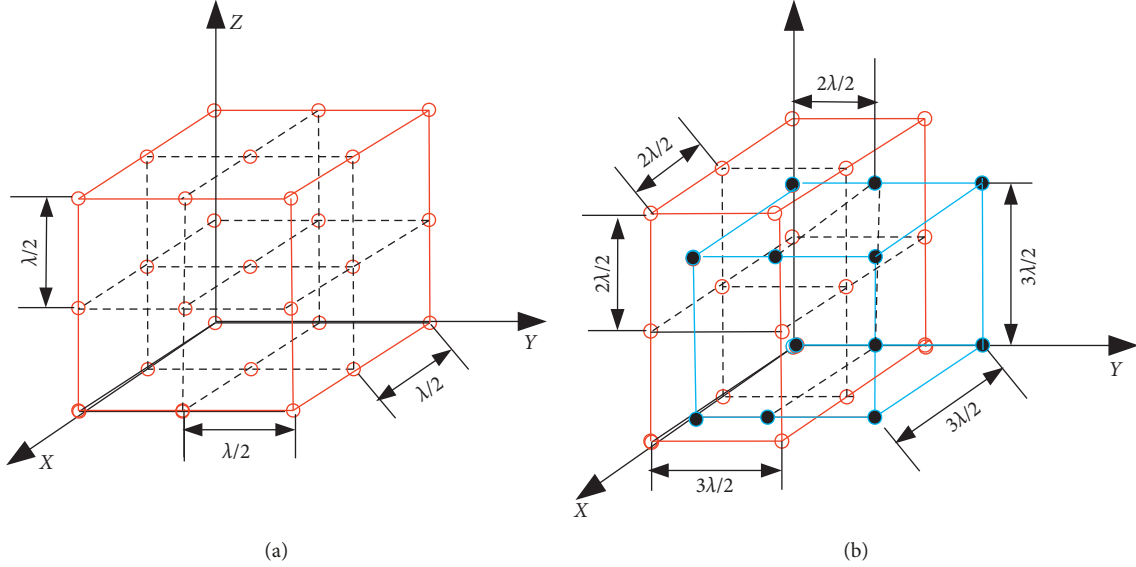


FIGURE 1: Array configurations. (a) The structure of UCA ( $M = N = J = 3$ ) and (b) the structure of CCA ( $M_1 = 3, N_1 = 2, J_1 = 3$  and  $M_2 = 2, N_2 = 3, J_2 = 2$ ).

TABLE 1: Performance of the array configurations.

Configuration	Total number of sensors	Array aperture	Coupling leakage
UCA	96	$5.625\lambda^3$	0.7588
CCA	89	$90\lambda^3$	0.2829

$k = 1, 2, \dots, K$ }, where  $\theta_k$  and  $\phi_k$  denote the DOA (the elevation angle and azimuth angle) of the  $k$ -th target [19]. And we define  $K < \min\{M_1 N_1 J_1, M_2 N_2 J_2\}$ ,  $u_k = \sin \theta_k \cos \phi_k \in (-1, 1)$ ,  $v_k = \sin \theta_k \sin \phi_k \in (0, 1)$ , and  $w_k = \cos \theta_k \in (0, 1)$ . In the following, we take the subarray that has  $M_i \times N_i \times J_i$  ( $i = 1, 2$ ) sensors to derive the proposed algorithm in the following part.

We denote the received signal as follows [28]:

$$\mathbf{x}_i(t) = \mathbf{A}_i \mathbf{s}(t) + \mathbf{n}_i(t), \quad i = 1, 2, \quad (7)$$

where  $\mathbf{s}(t) = [s_1(t), s_2(t), \dots, s_K(t)] \in \mathbb{C}^{K \times L}$  represents the signal matrix and  $L$  denotes the number of snapshots.  $\mathbf{n}_i \in \mathbb{C}^{M_i N_i J_i \times L}$  is the additive white Gaussian noise matrix, whose variance and mean are  $\sigma_n^2$  and zero, respectively.  $\mathbf{A}_i \in \mathbb{C}^{M_i N_i J_i \times K}$  denotes directional matrix of the  $i$ -th subarray and is presented by the following:

$$\mathbf{A}_i = \begin{bmatrix} \mathbf{a}_{x,i}(u_1) \otimes \mathbf{a}_{y,i}(v_1) \otimes \mathbf{a}_{z,i}(w_1), \dots, \mathbf{a}_{x,i}(u_K) \otimes \mathbf{a}_{y,i}(v_K) \\ \otimes \mathbf{a}_{z,i}(w_K) \end{bmatrix}, \quad (8)$$

where  $\mathbf{a}_{x,i}(u_k) = [1, e^{j2\pi d_{x,i} u_k / \lambda}, \dots, e^{j2\pi (M_i - 1) d_{x,i} u_k / \lambda}]^T$ ,  $\mathbf{a}_{y,i}(v_k) = [1, e^{j2\pi d_{y,i} v_k / \lambda}, \dots, e^{j2\pi (N_i - 1) d_{y,i} v_k / \lambda}]^T$  and  $\mathbf{a}_{z,i}(w_k) = [1, e^{j2\pi d_{z,i} w_k / \lambda}, \dots, e^{j2\pi (J_i - 1) d_{z,i} w_k / \lambda}]^T$  ( $k = 1, 2, \dots, K$ ) correspond to steering vectors of  $x$ -axis,  $y$ -axis, and  $z$ -axis of the subarray  $i$ .

Denote the directional matrix in (7) as follows:

$$\begin{aligned} \mathbf{A}_i &= \mathbf{A}_{x,i} \odot \mathbf{A}_{y,i} \odot \mathbf{A}_{z,i} \\ &= \begin{bmatrix} \mathbf{A}_{z,i} \mathbf{D}_1(\mathbf{A}_{y,i}) \mathbf{D}_1(\mathbf{A}_{x,i}) \\ \mathbf{A}_{z,i} \mathbf{D}_1(\mathbf{A}_{y,i}) \mathbf{D}_2(\mathbf{A}_{x,i}) \\ \vdots \\ \mathbf{A}_{z,i} \mathbf{D}_{N_i}(\mathbf{A}_{y,i}) \mathbf{D}_{M_i}(\mathbf{A}_{x,i}) \end{bmatrix}, \end{aligned} \quad (9)$$

where  $\mathbf{A}_{x,i}$  denotes directional matrix of  $x$ -axis of the subarray  $i$ , and  $\mathbf{A}_{y,i}, \mathbf{A}_{z,i}$  stand for the matrices of  $y$ -axis and  $z$ -axis, respectively,  $\mathbf{D}_n(\mathbf{A}_{y,i})$  ( $n = 1, 2, \dots, N$  and  $i = 1, 2$ ) denotes a diagonal matrix which is formed of the  $n$ -th row of the matrix  $\mathbf{A}_{y,i}$  for the subarray  $i$ , and  $\mathbf{D}_m(\mathbf{A}_{x,i})$  ( $m = 1, 2, \dots, M$  and  $i = 1, 2$ ) denotes a diagonal matrix which is formed of the  $m$ -th row of the matrix  $\mathbf{A}_{x,i}$  for the subarray  $i$ .

### 3. 2D DOA Estimation Algorithm

Conventional MD-MUSIC algorithm can obtain DOA estimates with high accuracy by selecting a refined search step, which causes expensive computational complexity. To tackle the problems, an AMRD-MUSIC algorithm is proposed.

3.1. MD-MUSIC Spectrum. We concatenate the array measurements  $\mathbf{x}_1(t)$  and  $\mathbf{x}_2(t)$  as follows:

$$\begin{aligned} \mathbf{x}(t) &= \begin{bmatrix} \mathbf{x}_1(t) \\ \mathbf{x}_2(t) \end{bmatrix} = \begin{bmatrix} \mathbf{A}_1 \\ \mathbf{A}_2 \end{bmatrix} \mathbf{s}(t) + \begin{bmatrix} \mathbf{n}_1(t) \\ \mathbf{n}_2(t) \end{bmatrix} \\ &= \mathbf{A} \mathbf{s}(t) + \mathbf{n}(t), \end{aligned} \quad (10)$$

where  $\mathbf{A} = [\mathbf{A}_1^T, \mathbf{A}_2^T]^T$  and  $\mathbf{n}(t) = [\mathbf{n}_1^T(t), \mathbf{n}_2^T(t)]^T$ .  $\mathbf{A}_1 \in \mathbb{C}^{M_1 N_1 J_1 \times K}$  and  $\mathbf{A}_2 \in \mathbb{C}^{M_2 N_2 J_2 \times K}$ . Then, the covariance matrix of the total array can be computed by the following:

$$\hat{R} = \frac{1}{L} \sum_{t=1}^L \mathbf{x}(t)\mathbf{x}^H(t) = \mathbf{U}_s \boldsymbol{\Sigma}_s \mathbf{U}_s^H + \mathbf{U}_n \boldsymbol{\Sigma}_n \mathbf{U}_n^H, \quad (11)$$

where  $\mathbf{U}_n \in \mathbb{C}^{(M_1 N_1 J_1 + M_2 N_2 J_2) \times (M_1 N_1 J_1 + M_2 N_2 J_2 - K)}$  refers to noise subspace and  $\mathbf{U}_s \in \mathbb{C}^{(M_1 N_1 J_1 + M_2 N_2 J_2) \times K}$  signifies signal subspace.  $\boldsymbol{\Sigma}_s \in \mathbb{C}^{K \times K}$  is a diagonal matrix with the  $K$  largest eigenvalues of  $\hat{R}$  and  $\boldsymbol{\Sigma}_n$  contains the remaining eigenvalues. Here, the symbol of  $(\hat{\cdot})$  means the estimation of the covariance matrix  $\mathbf{R}$ .

Then, according to 1D MUSIC spectrum [12], the MD-MUSIC spectrum can be solved as follows:

$$\begin{aligned} f(u, v, w) &= \frac{1}{\mathbf{a}^H(u, v, w) \mathbf{U}_n \mathbf{U}_n^H \mathbf{a}(u, v, w)} \\ &= \frac{1}{[\mathbf{a}_1^H(u, v, w) \mathbf{a}_2^H(u, v, w)] \mathbf{U}_n \mathbf{U}_n^H \begin{bmatrix} \mathbf{a}_1(u, v, w) \\ \mathbf{a}_2(u, v, w) \end{bmatrix}} \end{aligned} \quad (12)$$

**3.2. Array Mapping.** In this subsection, we utilize array mapping to extract two uniform arrays from the nonuniform array by exploiting the relation derived from the signal subspace and the two directional submatrices.

As the signal subspace spans the same space with the steering matrix doing, we have

where  $\mathbf{T} \in \mathbb{C}^{K \times K}$  represents a nonsingular matrix. Then, the signal subspace can be decomposed into two parts:

$$\mathbf{U}_s = \begin{bmatrix} \mathbf{A}_1 \\ \mathbf{A}_2 \end{bmatrix} \mathbf{T}, \quad (13)$$

where  $\mathbf{U}_{s1} \in \mathbb{C}^{M_1 N_1 J_1 \times K}$  and  $\mathbf{U}_{s2} \in \mathbb{C}^{M_2 N_2 J_2 \times K}$ .

Then, the transformation matrices can be defined as follows [38]:

$$\begin{aligned} \mathbf{H}_1 &= \mathbf{U}_{s2} \mathbf{U}_{s1}^+ = \mathbf{A}_2 \mathbf{T} \mathbf{T}^{-1} \mathbf{A}_1^+ = \mathbf{A}_2 \mathbf{A}_1^+, \\ \mathbf{H}_2 &= \mathbf{U}_{s1} \mathbf{U}_{s2}^+ = \mathbf{A}_1 \mathbf{T} \mathbf{T}^{-1} \mathbf{A}_2^+ = \mathbf{A}_1 \mathbf{A}_2^+, \end{aligned} \quad (15)$$

where  $(\cdot)^+$  denotes the pseudoinverse operation. From (15), we have the following:

$$\begin{aligned} \mathbf{A}_2 &= \mathbf{H}_1 \mathbf{A}_1, \\ \mathbf{A}_1 &= \mathbf{H}_2 \mathbf{A}_2, \end{aligned} \quad (16)$$

and the steering vectors of  $\mathbf{a}_1(u, v, w)$  and  $\mathbf{a}_2(u, v, w)$  also satisfy this relation in (16), so we have the following:

$$\begin{aligned} \mathbf{a}_2(u, v, w) &= \mathbf{H}_1 \mathbf{a}_1(u, v, w), \\ \mathbf{a}_1(u, v, w) &= \mathbf{H}_2 \mathbf{a}_2(u, v, w). \end{aligned} \quad (17)$$

By utilizing (17), we transform (13) into the following:

$$\begin{aligned} f_1(u, v, w) &= \frac{1}{[\mathbf{a}_1^H(u, v, w) \mathbf{a}_1^H(u, v, w) \mathbf{H}_1^H] \mathbf{U}_n \mathbf{U}_n^H \begin{bmatrix} \mathbf{a}_1(u, v, w) \\ \mathbf{H}_1 \mathbf{a}_1(u, v, w) \end{bmatrix}} \end{aligned} \quad (18)$$

$$\begin{aligned} &= \frac{1}{\mathbf{a}_1^H(u, v, w) \prod_1 \prod_1^H \mathbf{a}_1(u, v, w)}, \\ f_2(u, v, w) &= \frac{1}{[\mathbf{a}_2^H(u, v, w) \mathbf{H}_2^H \mathbf{a}_2^H(u, v, w)] \mathbf{U}_n \mathbf{U}_n^H \begin{bmatrix} \mathbf{H}_2 \mathbf{a}_2(u, v, w) \\ \mathbf{a}_2(u, v, w) \end{bmatrix}} \\ &= \frac{1}{\mathbf{a}_2^H(u, v, w) \prod_2 \prod_2^H \mathbf{a}_2(u, v, w)}, \end{aligned} \quad (19)$$

where  $\prod_1 = [\mathbf{I}_{M_1 N_1 J_1} \quad \mathbf{H}_1^H] \mathbf{U}_n$  and  $\prod_2 = [\mathbf{H}_2^H \quad \mathbf{I}_{M_2 N_2 J_2}] \mathbf{U}_n$ .

**3.3. Reduced Dimension Processing.** In this part, we employ the double reduced dimension processing on (16) and (17), respectively, to transform the 2D SPS into 1D one. Therefore, the computational complexity can be significantly reduced.

As  $\mathbf{a}_i(u, v, w) = \mathbf{a}_{x,i}(u) \otimes \mathbf{a}_{y,i}(v) \otimes \mathbf{a}_{z,i}(w) = \mathbf{a}_{x,i}(u) \otimes (\mathbf{a}_{y,i}(v) \otimes \mathbf{a}_{z,i}(w)) = (\mathbf{a}_{x,i}(u) \otimes \mathbf{I}_{N_i J_i}) (\mathbf{a}_{y,i}(v) \otimes \mathbf{a}_{z,i}(w))$ , then we have

$$\mathbf{a}_1(u, v, w) = (\mathbf{a}_{x,1}(u) \otimes \mathbf{I}_{N_1 J_1}) (\mathbf{a}_{y,1}(v) \otimes \mathbf{a}_{z,1}(w)), \quad (20)$$

$$\mathbf{a}_2(u, v, w) = (\mathbf{a}_{x,2}(u) \otimes \mathbf{I}_{N_2 J_2}) (\mathbf{a}_{y,2}(v) \otimes \mathbf{a}_{z,2}(w)), \quad (21)$$

where  $\mathbf{I}_{N_1 J_1}$  and  $\mathbf{I}_{N_2 J_2}$  are both identity matrices.

Then, we define the function  $\mathbf{Q}_i(u, v, w)$  ( $i = 1, 2$ ) as follows:

$$\mathbf{Q}_i(u, v, w) = \mathbf{a}_i^H(u, v, w) \prod_i \prod_i^H \mathbf{a}_i(u, v, w), \quad (22)$$

which transforms the 2D SPS to find the minimum value of (22). According to (20) and (21), we have the following:

$$\begin{aligned}
\mathbf{Q}_i(u, v, w) &= (\mathbf{a}_{x,i}(u) \otimes \mathbf{a}_{y,i}(v) \otimes \mathbf{a}_{z,i}(w))^H \prod_i \prod_i^H (\mathbf{a}_{x,i}(u) \otimes \mathbf{a}_{y,i}(v) \otimes \mathbf{a}_{z,i}(w)) \\
&= (\mathbf{a}_{x,i}(u) \otimes \mathbf{I}_{N_i J_i}) (\mathbf{a}_{y,i}(v) \otimes \mathbf{a}_{z,i}(w))^H \prod_i \prod_i^H ((\mathbf{a}_{x,i}(u) \otimes \mathbf{I}_{N_i J_i}) (\mathbf{a}_{y,i}(v) \otimes \mathbf{a}_{z,i}(w)))^H \\
&= (\mathbf{a}_{y,i}(v) \otimes \mathbf{a}_{z,i}(w))^H (\mathbf{a}_{x,i}(u) \otimes \mathbf{I}_{N_i J_i})^H \prod_i \prod_i^H (\mathbf{a}_{x,i}(u) \otimes \mathbf{I}_{N_i J_i}) (\mathbf{a}_{y,i}(v) \otimes \mathbf{a}_{z,i}(w)) \\
&= (\mathbf{a}_{y,i}(v) \otimes \mathbf{a}_{z,i}(w))^H \mathbf{G}_i(u) (\mathbf{a}_{y,i}(v) \otimes \mathbf{a}_{z,i}(w)) \\
&= \mathbf{f}_i^H(v, w) \mathbf{G}_i(u) \mathbf{f}_i(v, w),
\end{aligned} \tag{23}$$

where  $\mathbf{G}_i(u) = (\mathbf{a}_{x,i}(u) \otimes \mathbf{I}_{N_i J_i})^H \prod_i \prod_i^H (\mathbf{a}_{x,i}(u) \otimes \mathbf{I}_{N_i J_i})$ ,  $\mathbf{f}_i(v, w) = \mathbf{a}_{y,i}(v) \otimes \mathbf{a}_{z,i}(w)$ , and  $\mathbf{f}_i(v, w) \in \mathbb{C}^{N_i J_i \times 1}$ . Note that (23) is an optimization problem. Based on  $\mathbf{e}^H \mathbf{f}_i^H(v, w) = 1$ , where  $\mathbf{e} = [1, 0, \dots, 0]^T \in \mathbb{C}^{N_i J_i}$ , we can eliminate the trivial solution  $\mathbf{f}_i^H(v, w) = 0$ . This optimization problem can be reconstructed as follows:

$$\begin{aligned}
\min_{(u,v,w)} \quad & \mathbf{f}_i^H(v, w) \mathbf{G}_i(u) \mathbf{f}_i(v, w) \\
\text{s.t.} \quad & \mathbf{e}^H \mathbf{f}_i^H(v, w) = 1.
\end{aligned} \tag{24}$$

Then, we can construct the cost function as follows:

$$L(u, v, w) = \mathbf{f}_i^H(v, w) \mathbf{G}_i(u) \mathbf{f}_i(v, w) - \lambda (\mathbf{e}^H \mathbf{f}_i^H(v, w) - 1), \tag{25}$$

where  $\lambda$  is a constant. Then, we have the following:

$$\frac{\partial}{\partial \mathbf{f}(v, w)} L(u, v, w) = 2 \mathbf{G}_i(u) \mathbf{f}_i(v, w) + \lambda \mathbf{e}. \tag{26}$$

According to (26), we have  $\mathbf{f}_i(v, w) = \xi \mathbf{G}_i^{-1}(u) \mathbf{e}$ , where  $\xi$  is a constant. Combining (24), we have the following:

$$\xi = \frac{1}{\mathbf{e}^H \mathbf{G}_i^{-1}(u) \mathbf{e}}. \tag{27}$$

Then,  $\mathbf{f}_i(v, w)$  can be denoted as follows:

$$\mathbf{f}_i(v, w) = \frac{\mathbf{G}_i^{-1}(u) \mathbf{e}}{\mathbf{e}^H \mathbf{G}_i^{-1}(u) \mathbf{e}}. \tag{28}$$

Based on (24) and (28), we can obtain the following:

$$\hat{u}_k = \arg \min_u \frac{1}{\mathbf{e}^H \mathbf{G}_i^{-1}(u) \mathbf{e}} = \arg \max_u \mathbf{e}^H \mathbf{G}_i^{-1}(u) \mathbf{e}. \tag{29}$$

According to (29), the 2D SPS is transformed into 1D one by utilizing a reduced dimension process. To further reduce complexity, we employ the polynomial rooting technique with the lower computational complexity to obtain the final DOA estimates instead of the 1D SPS process.

**3.4. Polynomial Root Finding Process.** Define  $z_{x,i} = e^{-j2\pi d_i u / \lambda}$ , ( $i = 1, 2$ ) and denote  $\mathbf{a}_{x,i}(u)$  as follows:

$$\mathbf{a}_{x,i}(u) = \mathbf{a}(z_{x,i}) = [1, z_{x,i}, z_{x,i}^2, \dots, z_{x,i}^{M_i-1}]^T. \tag{30}$$

Then, we rewrite  $\mathbf{G}_i(u)$  as follows:

$$\mathbf{G}(z_{x,i}) = (\mathbf{a}^H(z_{x,i}) \otimes \mathbf{I}_{N_i J_i})^H \prod_i \prod_i^H (\mathbf{a}(z_{x,i}) \otimes \mathbf{I}_{N_i J_i}). \tag{31}$$

Then, we employ polynomial root finding technique instead of 1D SPS.

$$(\mathbf{a}^H(z_{x,i}) \otimes \mathbf{I}_{N_i J_i})^H \prod_i \prod_i^H (z_{x,i}) (\mathbf{a}(z_{x,i}) \otimes \mathbf{I}_{N_i J_i}) = 0. \tag{32}$$

If  $z_{x,i}$  cannot match with one source signal and if

$$\text{Rank}(\prod_i) \geq N_i J_i, \tag{33}$$

the matrix  $\prod_i$  is invertible [38].

In order to achieve the polynomial (32),  $z_{x,i}$  satisfies

$$\mathbf{D}(z_{x,i}) = \det(\prod_i(z_{x,i})) = 0. \tag{34}$$

Then, we can obtain the final  $\hat{u}_i^{(k)}$  by finding  $K$  roots which are closest to the unit circle of the polynomial  $\mathbf{D}(z_{x,i})$ ,  $z_{x,i}^k |_{k=1,2,\dots,K}$ ,

$$\hat{u}_i^{(k)} = \text{angle}(z_{x,i}^{(k)}) \frac{\lambda}{2\pi d_i}. \tag{35}$$

In order to obtain the estimation of  $\hat{v}_i^{(k)}$  or  $\hat{w}_i^{(k)}$ , the similar reduced dimensional polynomial root finding technique can be employed again. We can reform the whole steering matrix as  $\mathbf{A}_i' = [\mathbf{a}_{y,i}(v_1) \otimes \mathbf{a}_{x,i}(u_1) \otimes \mathbf{a}_{z,i}(w_1), \dots, \mathbf{a}_{y,i}(v_K) \otimes \mathbf{a}_{x,i}(u_K) \otimes \mathbf{a}_{z,i}(w_K)]$ , which contains the same elements as the matrix  $\mathbf{A}_i$  and only differs in elements positions. Then, a reconstructed received signal can be obtained. Then, we operate the proposed array mapping, reduced dimension, and polynomial rooting technique again to attain the estimate of  $\hat{v}_i^{(k)}$

$$\hat{v}_i^{(k)} = \text{angle}(z_{y,i}^{(k)}) \frac{\lambda}{2\pi d_i}. \tag{36}$$

Similarly, we can achieve  $\hat{w}_i^{(k)}$ . Phase ambiguity problem, resulting from the larger element spacing than half-wavelength, will be solved by coprime property in the following section.

3.5. *Ambiguity Elimination.* Firstly, the phase ambiguity problem is illustrated. Then, the coprime property is exploited to tackle the problem.

Assume that only one signal located with  $(\theta_\tau, \phi_\tau)$  impinges on the CCA subarray and the subarray consists of  $M_i \times N_i \times J_i$  sensors.  $(\theta_a, \phi_a)$  is assumed as one of the ambiguous DOAs of the real angle  $(\theta_\tau, \phi_\tau)$ .

According to [38],

$$\begin{cases} \text{mod}\left(\frac{2\pi}{\lambda}d_{xi}u_\tau\right) + 2k_u\pi = \frac{2\pi}{\lambda}d_{xi}u_\tau, \\ \text{mod}\left(\frac{2\pi}{\lambda}d_{yi}v_\tau\right) + 2k_v\pi = \frac{2\pi}{\lambda}d_{yi}v_\tau, \\ \text{mod}\left(\frac{2\pi}{\lambda}d_{zi}w_\tau\right) + 2k_w\pi = \frac{2\pi}{\lambda}d_{zi}w_\tau, \end{cases} \quad (37)$$

where the mod operation depends on the period of the exponential function  $2\pi$ . So it can be noted that the phase difference between the real and ambiguous DOAs is  $2k\pi$  ( $k \in \mathbb{Z}$ ) [39] and  $k_u, k_v, k_w \in \mathbb{Z}$  are integers. And  $d_{xi} = N_j\lambda/2$ ,  $d_{yi} = M_j\lambda/2$ ,  $d_{zi} = J_j\lambda/2$  ( $i, j \in [1, 2], i \neq j$ ) denote the element spacing among three axes, respectively.  $u_\tau = \sin \theta_\tau \cos \phi_\tau, v_\tau = \sin \theta_\tau \sin \phi_\tau, w_\tau = \cos \theta_\tau$ .

Then, we employ the obtained estimates to recover all estimates [28],

$$\frac{2\pi d_{xi}(u_\tau - u_a)}{\lambda} = 2k_u\pi, \quad (38)$$

$$\frac{2\pi d_{yi}(v_\tau - v_a)}{\lambda} = 2k_v\pi, \quad (39)$$

$$\frac{2\pi d_{zi}(w_\tau - w_a)}{\lambda} = 2k_w\pi, \quad (40)$$

where  $u_a = \sin \theta_a \cos \phi_a$ ,  $v_a = \sin \theta_a \sin \phi_a$ , and  $w_a = \cos \theta_a$  are defined and they denote the ambiguous values.

As  $\theta \in (0, \pi/2)$  and  $\phi \in (0, \pi)$ , we have  $u_a \in (-1, 1)$ ,  $v_a \in (0, 1)$ ,  $w_a \in (0, 1)$ . Simultaneously,  $u_a^2 + v_a^2 \in (0, 1)$  and  $u_a^2 + v_a^2 + w_a^2 = 1$  demand to satisfy each estimate.

As the interelement spacing of conventional UCA is limited to half-wavelength,  $k_u, k_v, k_w$  can only be the value of zero, which means no ambiguity problem exists. However, in CCA, due to the interelement spacing larger than half-wavelength, there are other pairs to make (37)–(39) hold besides the infeasible  $k_u, k_v$ , and  $k_w$  pairs, whereas only one pair is the candidate related to the actual DOA. Coprime property is utilized to solve the phase ambiguity problem and achieve true DOA.

Assume  $(\theta_a, \phi_a)$  as one of the ambiguous DOAs that appears in one of the subarrays. Simultaneously, define  $(\theta_i, \phi_i)$  as the corresponding actual DOA. There exists the following:

$$\begin{aligned} u_\tau - u_a &= \frac{2k_{ui}}{M_j}, \\ v_\tau - v_a &= \frac{2k_{vi}}{N_j}, \end{aligned} \quad (41)$$

$$w_\tau - w_a = \frac{2k_{wi}}{J_j}.$$

It exists that  $k_{ui} \in (-M_j, M_j)$ ,  $k_{vi} \in (-N_j/2, N_j/2)$ ,  $k_{wi} \in (-J_j/2, J_j/2)$ ,  $i, j \in \{1, 2\}, i \neq j$  [38], so we can obtain

$$\begin{aligned} \frac{k_{u1}}{M_2} &= \frac{k_{u2}}{M_1}, \\ \frac{k_{v1}}{N_2} &= \frac{k_{v2}}{N_1}, \\ \frac{k_{w1}}{J_2} &= \frac{k_{w2}}{J_1}. \end{aligned} \quad (42)$$

Since  $N_1, N_2, M_1, M_2$  and  $J_1, J_2$  are coprime integers pairs, respectively, (41) can hold only in the case of  $k_{u1} = k_{u2} = 0$ ,  $k_{v1} = k_{v2} = 0$ ,  $k_{w1} = k_{w2} = 0$ . It is indicated that the ambiguity problem is solved and actual DOA estimates can be achieved.

In practice, we only need two variables of  $(\hat{u}_k, \hat{v}_k, \hat{\gamma}_k)$  to achieve DOAs  $(\theta_k, \phi_k)$  estimates, where  $\hat{u}_k, \hat{v}_k, \hat{\gamma}_k$  are the estimates of  $u_k, v_k, \gamma_k$  ( $k = 1, 2, \dots, K$ ).

The final estimate of  $(\theta_k, \phi_k)$  can be calculated by the following:

$$\begin{aligned} \hat{\theta}_k &= \frac{\arcsin \sqrt{\hat{u}_k^2 + \hat{v}_k^2} + \arccos \hat{w}_k}{2}, \\ \hat{\phi}_k &= \frac{\arctan(\hat{u}_k/\hat{v}_k) + \arccos(\hat{u}_k/\sqrt{1 - \hat{w}_k^2})}{2}. \end{aligned} \quad (43)$$

3.6. *Detailed Steps of the Proposed Algorithm.* The steps are provided in detail as follows:

Step 1: compute the covariance of the received signal data to obtain the MD-MUSIC spectrum function (12).

Step 2: according to the signal subspace, construct  $\hat{H}_1$  and  $\hat{H}_2$  by (15), with which we can obtain the reconstructed spectrum function according to (19).

Step 3: by array mapping, we extract the two uniform arrays (19) from the nonuniform array (12) according to the relation derived from two directional matrices.

Step 4: according to (20) and (21), transform the 2D SPS process into 1D SPS.

Step 5: according to (32), convert 1D PSS to polynomial root finding process and obtain the  $K$  roots of  $\hat{u}_i^{(k)}$ . Similarly, we can achieve  $\hat{v}_i^{(k)}$  and  $\hat{w}_i^{(k)}$ .

Step 6: by (41), all the ambiguous DOA estimates are recovered, and by searching for the nearest ones, the actual estimations of  $u^{(k)}$ ,  $v^{(k)}$  and  $w^{(k)}$  can be achieved.

Step 7: according to (43), the final DOAs estimates can be obtained.

#### 4. Performance Analysis of the Algorithm

**4.1. DOF Comparison.** The proposed AMRD-MUSIC algorithm can obtain  $M_1N_1J_1 + M_2N_2J_2 - 1$  DOFs, which indicates that the proposed algorithm can achieve  $M_1N_1J_1 + M_2N_2J_2 - 2$  signals by employing  $M_1N_1J_1 + M_2N_2J_2 - 1$  antennas.

$$\text{DOF}_{\text{CCA}}^{\text{AMRD-MUSIC}} = M_1N_1J_1 + M_2N_2J_2 - 1. \quad (44)$$

The algorithms in [24, 26] process the two subarrays separately so that they have a great loss in DOFs since they only exploit the autoinformation. The number of achievable DOFs by using the method in [24, 26] can be denoted as follows:

$$\text{DOF}_{\text{CCA}}^{\text{algorithms in [24,26]}} = \min(M_1N_1J_1, M_2N_2J_2), \quad (45)$$

where  $M_1 = N_1 = J_1 > M_2 = N_2 = J_2$ .

Thus, the proposed algorithms can detect many more signals than conventional algorithms with the same sensors. From (44) and (45), we can note the relationship of DOFs of different algorithms as follows:

$$\text{DOF}_{\text{CCA}}^{\text{algorithms in [24,26]}} < \text{DOF}_{\text{CCA}}^{\text{AMRD-MUSIC}}. \quad (46)$$

Figure 2 depicts the maximum number of achievable DOFs to illustrate the signals explicitly without ambiguous DOA estimations, where the number of snapshots is set to be  $L = 500$  with noise-free, the total number of signals is  $K = 28$ , and the total number of sensors is  $T = 3 \times 2 \times 3 + 2 \times 3 \times 2 - 1 = 29$ . The elevation angles and azimuth angles are set to be  $\theta = [20^\circ, 20^\circ, 20^\circ, 20^\circ, 20^\circ, 20^\circ, 20^\circ, 20^\circ, 40^\circ, 40^\circ, 40^\circ, 40^\circ, 40^\circ, 40^\circ, 40^\circ, 60^\circ, 60^\circ, 60^\circ, 60^\circ, 60^\circ, 60^\circ, 60^\circ, 60^\circ, 80^\circ, 80^\circ, 80^\circ, 80^\circ, 80^\circ, 80^\circ]$  and  $\phi = [15^\circ, 25^\circ, 35^\circ, 45^\circ, 55^\circ, 65^\circ, 75^\circ, 15^\circ, 25^\circ, 35^\circ, 45^\circ, 55^\circ, 65^\circ, 75^\circ, 15^\circ, 25^\circ, 35^\circ, 45^\circ, 55^\circ, 65^\circ, 75^\circ, 15^\circ, 25^\circ, 35^\circ, 45^\circ, 55^\circ, 65^\circ, 75^\circ]$  respectively. From Figure 2, we can obviously see that the 28 signals can be detected uniquely due to the employment of total correlation matrix information including autocorrelation matrix and mutual correlation matrix, where no ambiguous angles arise; however, the methods in [24, 26] fail to detect 28 signals and they can detect 11 signals at most in this scenario.

**4.2. Complexity Analysis.** In this subsection, we compute the complexity of the classical MD-MUSIC algorithm, multiple-dimensional ESPRIT (MD-ESPRIT) algorithm and the proposed AMRD-MUSIC algorithm for the same array configuration of CCA with the same sensors.

For the MD-MUSIC algorithm, the total complexity is composed of three parts, including computing covariance, eigenvalues decomposition, and spectrum peak searching. The complexity of these three parts is presented as  $T^2L$ ,  $T^3$  and  $(180/\tau)(90/\tau)[T(T-K)]$ , respectively, where  $L$

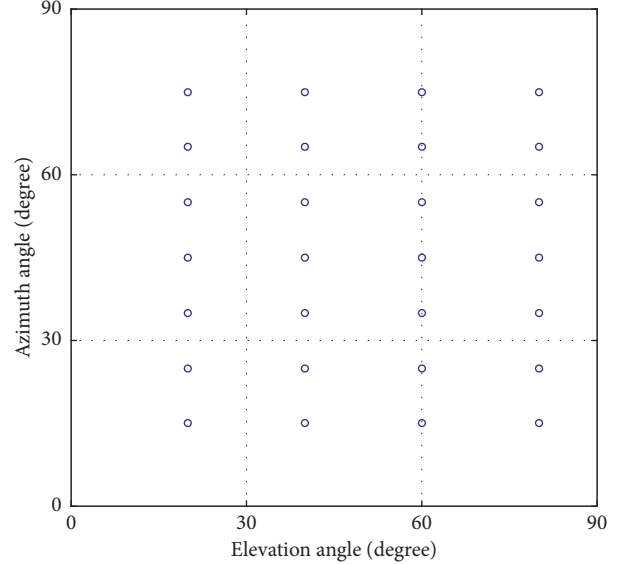


FIGURE 2: Maximum achievable DOFs without ambiguous angles by using the AMRD-MUSIC algorithm.

represents the number of snapshots  $T = T_1 + T_2$ ,  $T_1 = M_1N_1J_1$ ,  $T_2 = M_2N_2J_2$  and  $\tau$  denotes the searching step. So the total computational complexity can be denoted as  $T^2L + T^3 + (180/\tau)(90/\tau)[T(T-K)]$ .

And we compute the complexity of the MD-ESPRIT algorithm. For the two subarrays, complexity consists of three parts, computing the covariance as  $T^2L$ , eigenvalue decomposition as  $T_1^3 + T_2^3$ , computing pseudoinverse and eigenvalue decomposition after reconstruction as  $(T_1 - N_1J_1)^3 + (T_2 - N_2J_2)^3 + (T_1 - M_1J_1)^3 + (T_2 - M_2J_2)^3 + (T_1 - N_1M_1)^3 + (T_2 - N_2M_2)^3$ . So the total complexity of these operations is denoted as  $T^2L + T_1^3 + T_2^3 + (T_1 - N_1J_1)^3 + (T_2 - N_2J_2)^3 + (T_1 - M_1J_1)^3 + (T_2 - M_2J_2)^3 + (T_1 - N_1M_1)^3 + (T_2 - N_2M_2)^3$ .

In the proposed AMRD-MUSIC algorithm, the complexity can be denoted as  $T_1^2L + 2KT_1T_2 + 2T_1T_2^2 + 2N_1J_1T_1T + (N_1J_1)^2T_1 + (T - N_1J)^3 + 2N_2J_2T_2T + (N_2J_2)^2T_2 + T_2^3$ , and the complexity of the other subarray is approximately similar to it.

We compare the complexity of the conventional MD-MUSIC algorithm, the MD-ESPRIT algorithm, and the proposed AMRD-MUSIC algorithm with the same CCA configuration. For clarity, we list the computational complexity of these algorithms with CCA in Table 2 with  $L = 200$ ,  $K = 2$ ,  $M_1 = 3$ ,  $M_2 = 2$ ,  $N_1 = 2$ ,  $N_2 = 3$ ,  $J_1 = 3$ ,  $J_2 = 2$ ,  $J_1 = 3$ ,  $J_2 = 2$ , and the searching step  $\tau$  is set to be 0.02.

We compare the computational complexity versus the number of snapshots and sensors respectively of three algorithms including MD-MUSIC, MD-ESPRIT, and ARMD-MUSIC. Figures 3 and 4 show the complexity comparison with the increasing number of snapshots and sensors, respectively. It can be seen that the proposed AMRD-MUSIC algorithm achieves the lowest computational complexity than other algorithms. Figure 5 shows the complexity comparison versus the searching step. We can see that the complexity of MD-MUSIC reduces with the searching step

TABLE 2: Computational complexity of different algorithms.

Algorithms	Complex multiplication
MD-MUSIC	$5.4432 \times 10^9$
MD-ESPRIT	$1.9212 \times 10^5$
AMRD-MUSIC	$1.20096 \times 10^5$

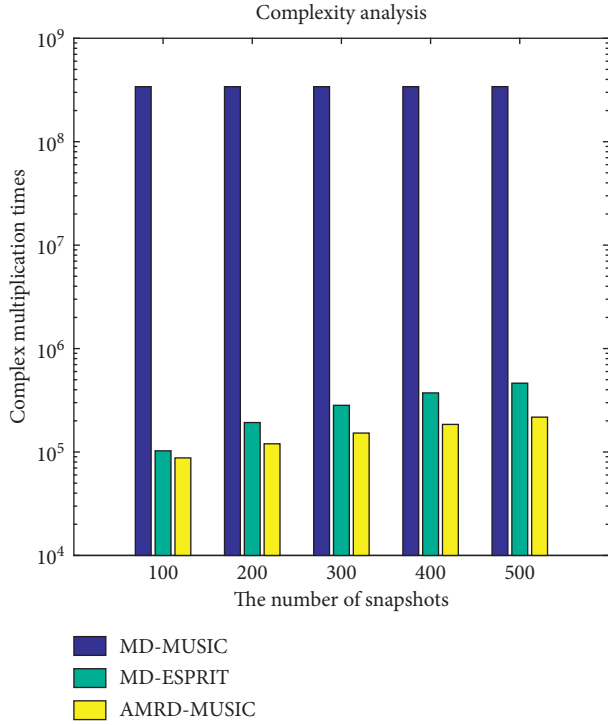


FIGURE 3: Comparison of total complexity versus snapshots.

increasing. However, the proposed AMRD-MUSIC algorithm outperforms the other algorithms.

4.3. *Advantages of the Proposed Algorithm.* In summary, the advantages of the proposed algorithm are listed as follows:

- (1) The proposed algorithm achieves significant complexity decrease by reducing 2D SPS into 1D one and utilizing polynomial root finding technique instead of 1D SPS.
- (2) The proposed algorithm possesses approximately the same DOA estimation performance as the MD-MUSIC algorithm and behaves better in its estimation than the classic MD-ESPRIT algorithm.
- (3) The proposed algorithm can obtain full DOFs due to the utilization of the total matrix information.
- (4) The proposed algorithm can achieve DOA angles with pairing automatically.

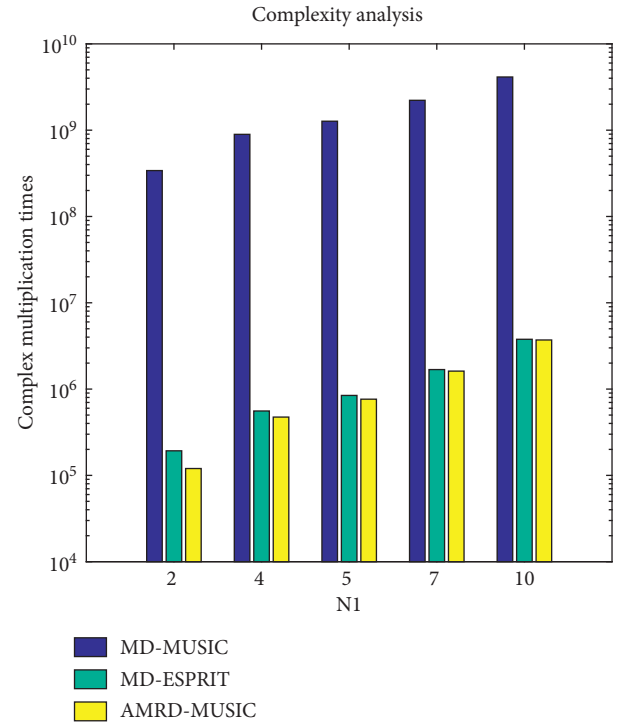


FIGURE 4: Comparison of total complexity versus the number of elements.

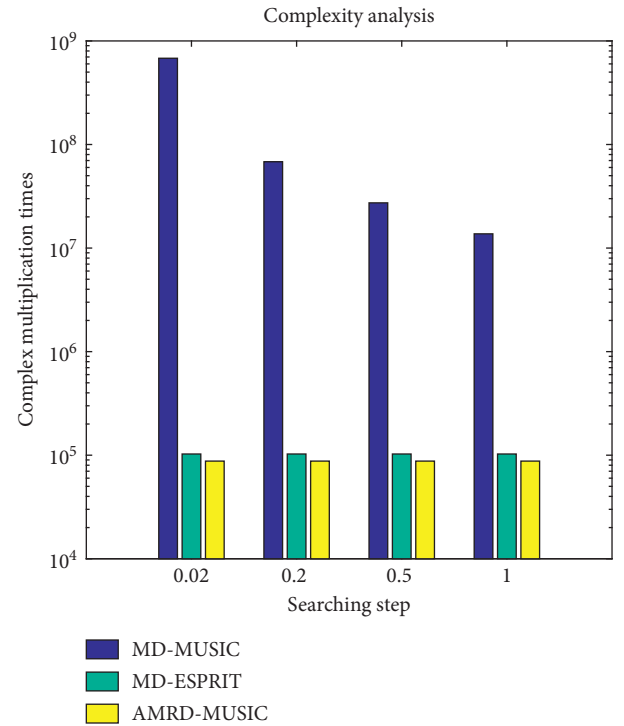


FIGURE 5: Comparison of total complexity versus searching step.

**4.4. Cramer–Rao Bound.** We provide the Cramer–Rao Bound (CRB) [40–42] analytical derivation of DOA estimation for CCA. The signal covariance can be obtained by the following:

$$\mathbf{R}_s = \frac{1}{L} \sum_{t=1}^L \mathbf{s}(t)\mathbf{s}^H(t), \quad (47)$$

and we define the matrix parameter vector  $\boldsymbol{\eta} = [\theta_1, \theta_2, \dots, \theta_K, \phi_1, \phi_2, \dots, \phi_K]^T$ .

Then, we can denote the  $(\xi_0, \zeta_0)$ -th element of the Fisher information matrix (FIM) as follows [42]:

$$\begin{aligned} \text{FIM}_{(\xi_0, \zeta_0)} &= \varsigma_0 \text{tr} \left( \frac{\partial \bar{\mathbf{p}}}{\partial \eta_{\xi_0}} \mathbf{P}^{-1} \frac{\partial \bar{\mathbf{p}}}{\partial \eta_{\zeta_0}} \mathbf{P}^{-1} \right) \\ &= \varsigma_0 \left( \frac{\partial \bar{\mathbf{p}}}{\partial \eta_{\xi_0}} \right)^H (\mathbf{P}^T \otimes \mathbf{P})^{-1} \frac{\partial \bar{\mathbf{p}}}{\partial \eta_{\zeta_0}}, \end{aligned} \quad (48)$$

where

$$\varsigma_0 = M_1 N_1 J_1 + M_2 N_2 J_2, \quad (49)$$

$$\mathbf{P} = \mathbf{A} \mathbf{P}_s \mathbf{A}^H + \mathbf{I}_{\varsigma_0}, \quad (50)$$

$$\bar{\mathbf{p}} = \text{vec}(\mathbf{P}) = (\mathbf{A}^* \circ \mathbf{A}) \boldsymbol{\Xi} + \text{vec}(\mathbf{I}_{\varsigma_0}), \quad (51)$$

and we denote  $\partial \bar{\mathbf{p}} / \partial \boldsymbol{\eta} = [\partial \bar{\mathbf{p}} / \partial \theta_1, \partial \bar{\mathbf{p}} / \partial \theta_2, \dots, \partial \bar{\mathbf{p}} / \partial \theta_K, \partial \bar{\mathbf{p}} / \partial \phi_1, \partial \bar{\mathbf{p}} / \partial \phi_2, \dots, \partial \bar{\mathbf{p}} / \partial \phi_K]$ ; then we have the following:

$$\text{FIM} = \varsigma_0 \left( \frac{\partial \bar{\mathbf{p}}}{\partial \boldsymbol{\eta}} \right)^H (\mathbf{P}^T \otimes \mathbf{P})^{-1} \frac{\partial \bar{\mathbf{p}}}{\partial \boldsymbol{\eta}}. \quad (52)$$

By utilizing (52), we can calculate the following:

$$\frac{\partial \bar{\mathbf{p}}}{\partial \boldsymbol{\eta}} = [\mathbf{A}_{d1} \boldsymbol{\Pi}, \mathbf{A}_{d2} \boldsymbol{\Pi}], \quad (53)$$

where

$$\mathbf{A}_{d1} = (\mathbf{D}_1^* \circ \mathbf{A} + \mathbf{A}^* \circ \mathbf{D}_1),$$

$$\mathbf{A}_{d2} = (\mathbf{D}_2^* \circ \mathbf{A} + \mathbf{A}^* \circ \mathbf{D}_2),$$

$$\mathbf{D}_1 = \left[ \frac{\partial \mathbf{a}(u_1, v_1)}{\partial \theta_1}, \frac{\partial \mathbf{a}(u_2, v_2)}{\partial \theta_2}, \dots, \frac{\partial \mathbf{a}(u_K, v_K)}{\partial \theta_K} \right],$$

$$\mathbf{D}_2 = \left[ \frac{\partial \mathbf{a}(u_1, v_1)}{\partial \phi_1}, \frac{\partial \mathbf{a}(u_2, v_2)}{\partial \phi_2}, \dots, \frac{\partial \mathbf{a}(u_K, v_K)}{\partial \phi_K} \right],$$

$$\mathbf{a}(u_k, v_k) = \begin{bmatrix} \mathbf{a}_{x1}(u_k) \otimes \mathbf{a}_{y1}(v_k) \otimes \mathbf{a}_{z1}(w_k) \\ \mathbf{a}_{x2}(u_k) \otimes \mathbf{a}_{y2}(v_k) \otimes \mathbf{a}_{z2}(w_k) \end{bmatrix}, \quad k = 1, 2, \dots, K,$$

$$\boldsymbol{\Pi} = \text{diag}(\boldsymbol{\Xi}).$$

(54)

The matrix  $\mathbf{P}^T \otimes \mathbf{P}$  is positive definite since the  $\mathbf{P}$  in (50) is positive definite.

By letting

$$\mathbf{F} = (\mathbf{P}^T \otimes \mathbf{P})^{-1/2} \mathbf{A}_d \mathbf{R}_0, \quad (55)$$

the CRB can be obtained as follows:

$$\text{CRB} = \frac{1}{\varsigma_0} (\mathbf{F}^H \mathbf{F})^{-1}, \quad (56)$$

where  $\mathbf{A}_d = [\mathbf{A}_{d1}, \mathbf{A}_{d2}]$ ,  $\mathbf{R}_0 = \text{diag}(\mathbf{R}_s, \mathbf{R}_s)$ .

## 5. Simulation Results

Numerical simulations are provided to evaluate the performance of the proposed array configuration of CCA and algorithm in this part. For the CCA geometry, it consists of two uniform cubic subarrays of  $3 \times 2 \times 3$  and  $2 \times 3 \times 2$  sensors, where  $d_{x1} = 2\lambda/2$ ,  $d_{y1} = 3\lambda/2$ ,  $d_{z1} = 2\lambda/2$ ,  $d_{x2} = 3\lambda/2$ ,  $d_{y2} = 2\lambda/2$ , and  $d_{z2} = 3\lambda/2$ . The total number of these two subarrays is computed as  $T = 3 \times 2 \times 3 + 2 \times 3 \times 2 - 1 = 29$ . The UCA consists of  $3 \times 2 \times 5 = 30$  sensors. Assume  $K = 2$  signals impinging on the arrays from  $(\theta_1, \phi_1) = (20^\circ, 30^\circ)$  and  $(\theta_2, \phi_2) = (50^\circ, 70^\circ)$ . From Figure 6, we can clearly see that the AMRD-MUSIC algorithm is able to detect the DOA targets successfully.

The root mean square error (RMSE), as the performance metric of the DOA estimation, is defined as follows:

$$\text{RMSE} = \sqrt{\frac{1}{\text{PK}} \sum_{p=1}^P \sum_{k=1}^K \left( (\theta_k - \hat{\theta}_k^p)^2 + (\phi_k - \hat{\phi}_k^p)^2 \right)}, \quad (57)$$

where  $K$  is the number of sources.  $(\hat{\theta}_k^p, \hat{\phi}_k^p)$  ( $k = 1, 2, \dots, K$ ) are estimates of  $(\theta_k, \phi_k)$  of the  $p$ -th Monte Carlo trial, respectively. In this paper, we set  $P = 500$ .

**5.1. DOA Estimation Performance Comparison of Different Array Configurations with the Same Algorithm.** We employ simulations to illustrate the DOA estimation performance of UCA and CCA configurations by using the same algorithm, where.  $K = 2$ ,  $(\theta_1, \phi_1) = [15^\circ, 30^\circ]$ ,  $(\theta_2, \phi_2) = [20^\circ, 40^\circ]$ .

Figures 7 and 8 exhibit the RMSE performance comparison between CCA and UCA by utilizing the same algorithm. It captures explicitly that the proposed AMRD-MUSIC algorithm with CCA possesses better DOA estimation performance because of the extended array aperture and less MC effects. And CRB comparison shows that CCA can obtain the lower bound of theoretical DOA estimation performance compared with UCA geometry.

**5.2. DOA Estimation Performance Comparison of Different Algorithms with the Same Array.** In this subsection, we compare the RMSE performance of different algorithms with the same array of CCA, including the proposed AMRD-MUSIC algorithm, conventional MD-MUSIC algorithm, and MD-ESPRIT algorithm.

Figures 9 and 10 present the 2D angle estimation comparisons versus SNR and  $L$ , respectively. The two figures clearly show that the proposed AMRD-MUSIC algorithm has approximately the same DOA estimation performance as the MD-MUSIC algorithm and

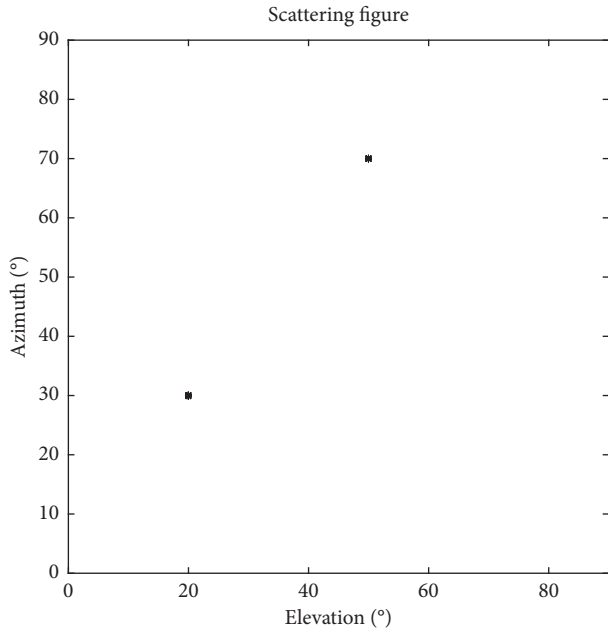


FIGURE 6: Scattering figure with AMRD-MUSIC for CCA.

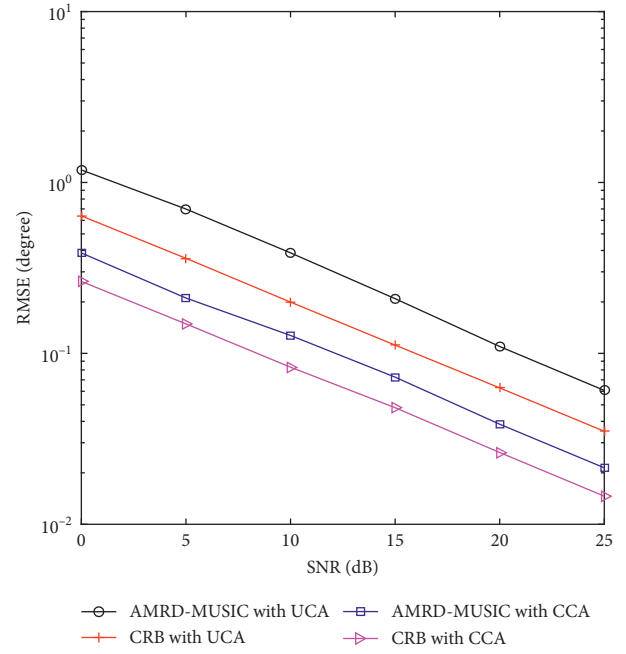


FIGURE 8: RMSE of different arrays versus SNR.

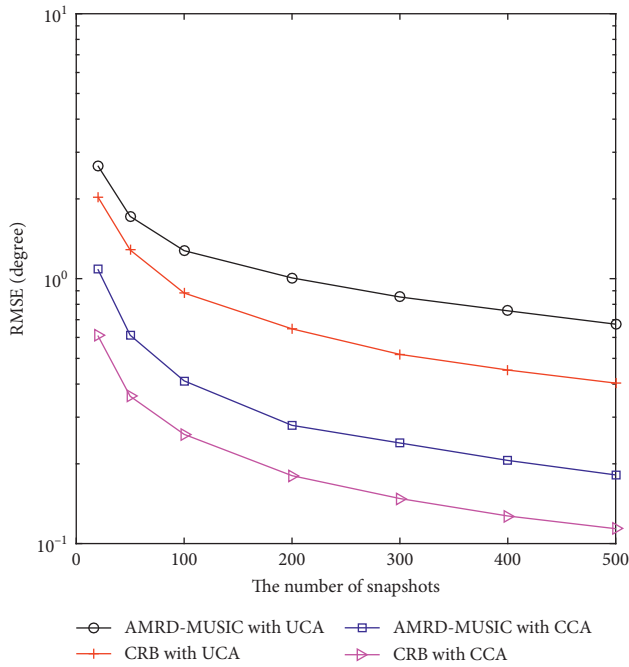


FIGURE 7: RMSE of different arrays versus snapshots.

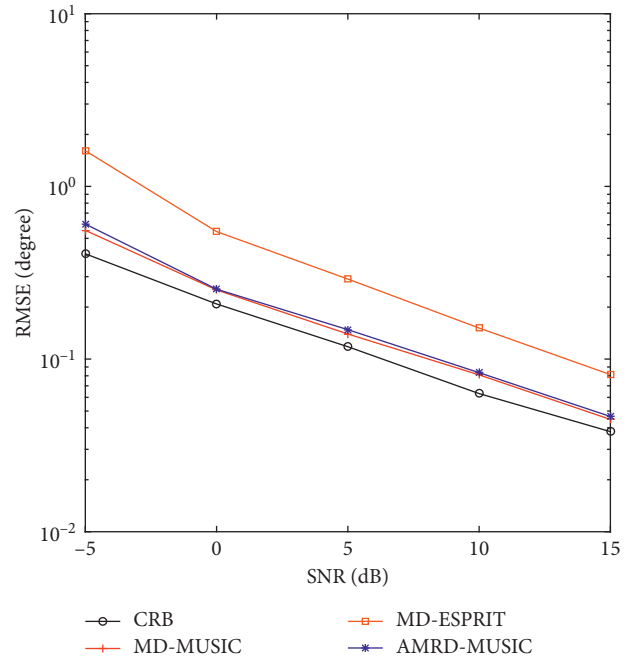


FIGURE 9: RMSE comparison of different algorithms versus SNR.

outperforms the classic MD-ESPRIT algorithm owing to the utilization of total information including autocorrelation matrix and mutual correlation matrix, while the proposed algorithm has a lower computational complexity as shown in Figure 2.

*5.3. Comparison of DOA Estimation Performance versus the Number of Sensors.* In this subsection, we employ the proposed approach to a CCA geometry which consists of two subarrays including  $3 \times N \times 3$  and  $2 \times 3 \times 2$  sensors, where  $N = [2, 4, 5]$ . The RMSE performance versus SNR and snapshots are displayed in Figures 11 and 12, respectively. It is

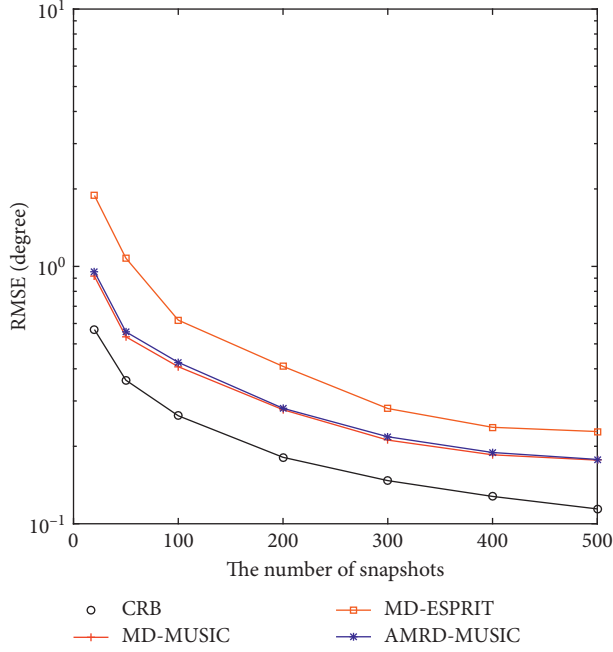


FIGURE 10: RMSE comparison of different algorithms versus snapshots.

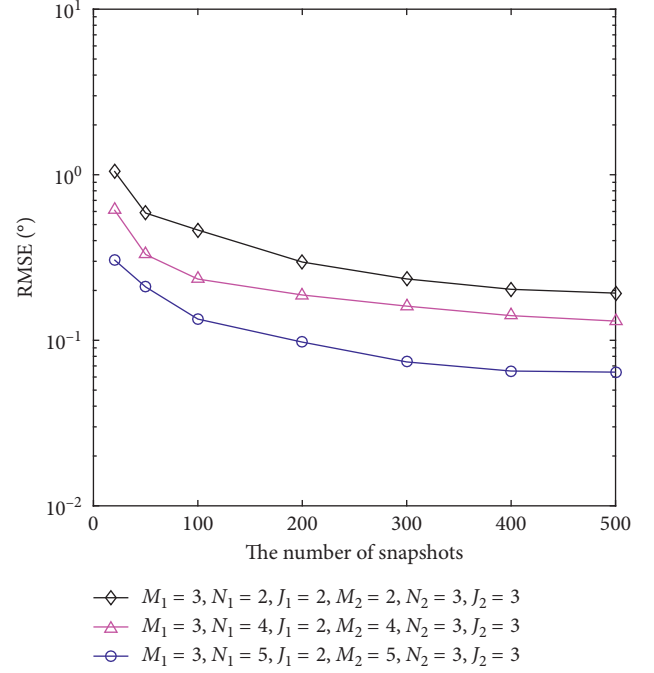


FIGURE 12: RMSE performance of different number of sensors versus snapshots.

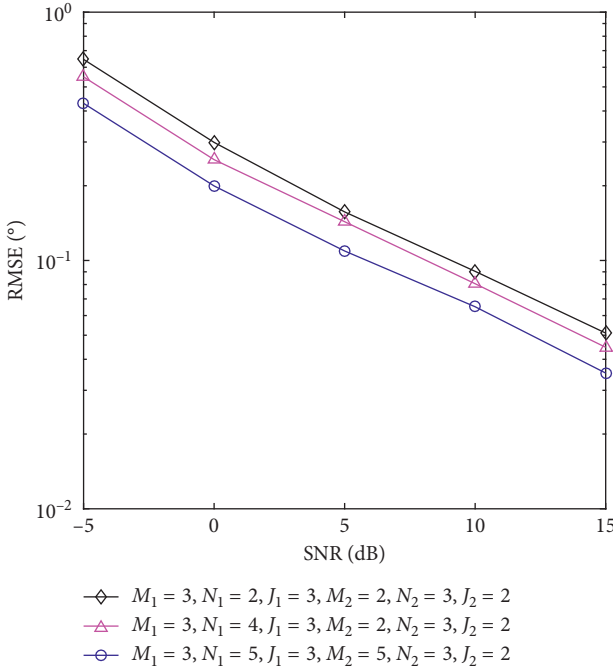


FIGURE 11: RMSE performance of different number of sensors versus SNR.

obviously shown that the RMSE estimation performance of the proposed AMRD-MUSIC algorithm is improving with the increase of SNR or snapshots due to the diversity gain.

## 6. Conclusions

In this paper, a CCA geometry in massive MIMO systems is constructed, which consists of two uniform cubic subarrays and obtains the extension of interelement spacing by selecting three pairs of coprime integers. Meanwhile, CRB for CCA is derived and the proposed CCA geometry is verified to outperform the conventional UCA geometry in 2D DOA estimation performance in massive MIMO systems. In addition, we propose a computationally efficient 2D DOA estimation algorithm via array mapping and reduced dimension for CCA. In the proposed algorithm, we utilize the array mapping and map the nonuniform array into two uniform arrays and operate the reduced dimension process on the two uniform arrays to transform the 2D SPS problem into 1D one. In addition, the computational complexity gets further reduced by converting the 1D SPS problem into a polynomial root finding problem. Numerical simulation results verify the effectiveness of the proposed algorithm that can reduce the computational complexity cost with no degradation of DOA estimation performance.

## Data Availability

No data were used to support this study.

## Conflicts of Interest

The authors declare that they have no conflicts of interest.

## Acknowledgments

This work was supported by the China NSF Grants (61971217, 61371169, 61601167), Shandong Province NSF Grants (ZR2016FM43), Key Laboratory of Dynamic Cognitive System of Electromagnetic Spectrum Space (Nanjing University of Aeronautics and Astronautics), and Ministry of Industry and Information Technology (KF20181915).

## References

- [1] H. Q. Ngo, E. G. Larsson, and T. L. Marzetta, "Energy and spectral efficiency of very large multiuser MIMO systems," *IEEE Transactions on Communications*, vol. 61, no. 4, pp. 1436–1449, 2013.
- [2] Y. Huang, S. He, S. Jin, and W. Chen, "Decentralized energy-efficient coordinated beamforming for multicell systems," *IEEE Transactions on Vehicular Technology*, vol. 63, no. 9, pp. 4302–4314, 2014.
- [3] X. Gao, L. Dai, S. Han, C.-L. I, and R. W. Heath, "Energy-efficient hybrid analog and digital precoding for mmwave MIMO systems with large antenna arrays," *IEEE Journal on Selected Areas in Communications*, vol. 34, no. 4, pp. 998–1009, 2016.
- [4] J. Zuo, J. Zhang, C. Yuen, W. Jiang, and W. Luo, "Energy-efficient downlink transmission for multicell massive DAS with pilot contamination," *IEEE Transactions on Vehicular Technology*, vol. 66, no. 2, pp. 1209–1221, 2017.
- [5] E. G. Larsson, O. Edfors, F. Tufvesson, and T. L. Marzetta, "Massive MIMO for next generation wireless systems," *IEEE Communications Magazine*, vol. 52, no. 2, pp. 186–195, 2014.
- [6] Y. Z. Su, X. W. Liu, D. Y. Li, X. B. Wang, and Y. H. Zhang, "Research on impact localization in composite materials using array signal processing and lamb wave," *Advanced Materials Research*, vol. 304, pp. 65–72, 2011.
- [7] X. Zhang, L. Xu, L. Xu, and D. Xu, "Direction of departure (DOD) and direction of arrival (DOA) estimation in MIMO radar with reduced-dimension MUSIC," *IEEE Communications Letters*, vol. 14, no. 12, pp. 1161–1163, 2010.
- [8] J. Wang, J. Chen, and D. Cabric, "Cramer-rao bounds for joint RSS/DoA-Based primary-user localization in cognitive radio networks," *IEEE Transactions on Wireless Communications*, vol. 12, no. 3, pp. 1363–1375, 2013.
- [9] X. Wang, W. Wang, X. Li, and J. Liu, "Real-valued covariance vector sparsity-inducing DOA estimation for monostatic MIMO radar," *Sensors*, vol. 15, no. 11, pp. 28271–28286, 2015.
- [10] S. Marcos, A. Marsal, and M. Benidir, "The propagator method for source bearing estimation," *Signal Processing*, vol. 42, no. 2, pp. 121–138, 1995.
- [11] J. Capon, "High-resolution frequency-wavenumber spectrum analysis," *Proceedings of the IEEE*, vol. 57, no. 8, pp. 1408–1418, 1969.
- [12] R. Schmidt, "Multiple emitter location and signal parameter estimation," *IEEE Transactions on Antennas and Propagation*, vol. 34, no. 3, pp. 276–280, 1986.
- [13] R. Roy and T. Kailath, "ESPRIT-estimation of signal parameters via rotational invariance techniques," *IEEE Transactions on Acoustics Speech and Signal Processing*, vol. 37, no. 7, pp. 984–995, 2002.
- [14] M. Pesavento, A. B. Gershman, and M. Haardt, "Unitary root-MUSIC with a real-valued eigen-decomposition: a theoretical and experimental performance study," *IEEE Transactions on Signal Processing*, vol. 48, no. 5, pp. 1306–1314, 2000.
- [15] X. Zhang, H. Wu, J. Li, and D. Xu, "Computationally efficient DOD and DOA estimation for bistatic MIMO radar with propagator method," *International Journal of Electronics*, vol. 99, no. 9, pp. 1207–1221, 2012.
- [16] F. Gao and A. B. Gershman, "A generalized ESPRIT approach to direction-of-arrival estimation," *IEEE Signal Processing Letters*, vol. 12, no. 3, pp. 254–257, 2005.
- [17] H. Chen, C. Hou, Q. Wang, L. Huang, W. Yan, and L. Pu, "Improved azimuth/elevation angle estimation algorithm for three-parallel uniform linear arrays," *IEEE Antennas and Wireless Propagation Letters*, vol. 14, pp. 329–332, 2015.
- [18] C. P. Huang and M. D. Zoltowski, "Eigenstructure techniques for 2-D angle estimation with uniform circular array," *IEEE Transactions on Signal Processing*, vol. 42, no. 9, pp. 2395–2407, 1994.
- [19] X. Zhang, W. Zheng, W. Chen, and Z. Shi, "Two-dimensional DOA estimation for generalized coprime planar arrays: a fast-convergence trilinear decomposition approach," *Multidimensional Systems and Signal Processing*, vol. 30, no. 1, pp. 239–256, 2019.
- [20] P. Pal and P. P. Vaidyanathan, "Sparse sensing with coprime samplers and arrays," *IEEE Transactions on Signal Processing*, vol. 59, no. 2, pp. 573–586, 2011.
- [21] S. Qin, Y. D. Zhang, and M. G. Amin, "Generalized coprime array configurations for direction-of-arrival estimation," *IEEE Transactions on Signal Processing*, vol. 63, no. 6, pp. 1377–1390, 2015.
- [22] P. Pal and P. P. Vaidyanathan, "Coprime sampling and the music algorithm," *Digital Signal Processing Workshop and IEEE Signal Processing Education Workshop*, pp. 289–294, 2011.
- [23] Z. Ye and C. Liu, "2D DOA estimation in the presence of mutual coupling," *IEEE Transactions on Antennas and Propagation*, vol. 56, no. 10, pp. 3150–3158, 2008.
- [24] C. Zhou, Z. Shi, Y. Gu, and X. Shen, "DECOM: DOA estimation with combined MUSIC for coprime array," *IEEE International Conference on Wireless Communication and Signal Processing (WCSP)*, pp. 1–5, 2013.
- [25] W. Zheng, X. F. Zhang, P. Gong, and H. Zhai, "DOA estimation for coprime linear arrays: an ambiguity-free method involving full DOFs," *IEEE Communication Letters*, vol. 22, no. 3, pp. 562–565, 2018.
- [26] F. Sun, B. Gao, and P. Lan, "Partial spectral search based DOA estimation method for co-prime linear arrays," *Electronics Letters*, vol. 51, no. 24, pp. 2053–2055, 2015.
- [27] D. Zhang, Y. Zhang, G. Zheng, C. Feng, and J. Tang, "Improved DOA estimation algorithm for co-prime linear arrays using root-MUSIC algorithm," *Electronics Letters*, vol. 53, no. 18, pp. 1277–1279, 2017.
- [28] Q. Wu, F. Sun, P. Lan, G. Ding, and X. Zhang, "Two-dimensional direction-of-arrival estimation for co-prime planar arrays: a partial spectral search approach," *IEEE Sensors Journal*, vol. 16, no. 14, pp. 5660–5670, 2016.
- [29] Z. Wang, Z. Xiaofei, and S. Zhan, "Two-dimensional direction of arrival estimation for coprime planar arrays via a computationally efficient one-dimensional partial spectral search approach," *IET Radars and Sonar Navigation*, vol. 11, no. 10, pp. 1581–1588, 2017.
- [30] W. Zheng, X. Zhang, and H. Zhai, "Generalized coprime planar array geometry for 2-D DOA estimation," *IEEE Communications Letters*, vol. 21, no. 5, pp. 1075–1078, 2017.
- [31] L. Xu, J. Li, and P. Stoica, "Target detection and parameter estimation for MIMO radar systems," *IEEE Transactions on*

- Aerospace and Electronic Systems*, vol. 44, no. 3, pp. 927–939, 2008.
- [32] L. Wan, G. Han, J. Jiang, J. J. P. C. Rodrigues, N. Feng, and T. Zhu, “DOA estimation for coherently distributed sources considering circular and noncircular signals in massive MIMO systems,” *IEEE Systems Journal*, vol. 11, no. 1, pp. 41–49, 2017.
- [33] D. Nion and N. D. Sidiropoulos, “Adaptive algorithms to track the PARAFAC decomposition of a third order tensor,” *IEEE Transactions on Signal Processing*, vol. 57, no. 6, pp. 2299–2310, 2009.
- [34] Y. Doi, K. Ichige, H. Arai et al., “3-D array configuration using multiple regular tetrahedra for high-resolution 2-D DOA estimation,” *IEEE Signal Processing Conference*, pp. 1955–1959, 2014, <http://ieeexplore.ieee.org/stamp/stamp.jsp?tp=&arnumber=6952711&isnumber=6951911>.
- [35] H. Moriya, K. Ichige, H. Arai, T. Hayashi, H. Matsuno, and M. Nakano, “Improving elevation estimation accuracy in DOA: how planar arrays can be modified into 3-D configuration,” *IEICE Transactions on Fundamentals*, vol. E95.A, no. 10, pp. 1658–1666, 2012.
- [36] D. Bernard, *Principles of Aperture and Array System Design*, Wiley, Hoboken, NJ, USA, 1976.
- [37] J. Liu, Y. Zhang, Y. Lu et al., “Augmented nested arrays with enhanced DOF and reduced mutual coupling,” *IEEE Transactions on Signal Processing*, vol. 65, no. 21, pp. 5549–5563, 2017.
- [38] D. Zhang, Y. Zhang, G. Zheng, B. Deng, C. Feng, and J. Tang, “Two-dimensional direction of arrival estimation for coprime planar arrays via polynomial root finding technique,” *IEEE Access*, vol. 6, pp. 199540–219549, 2018.
- [39] D. Tse and P. Viswanath, *Fundamentals of Wireless Communication*, Cambridge University Press, Cambridge, UK, 2005.
- [40] P. Stoica and A. Nehorai, “MUSIC, maximum likelihood, and Cramer-Rao bound,” *IEEE Transactions on Acoustics, Speech, and Signal Processing*, vol. 37, no. 5, pp. 720–741, 1989.
- [41] P. Stoica and A. Nehorai, “MUSIC, maximum likelihood, and Cramer-Rao bound: further results and comparisons,” *IEEE Transactions on Acoustics, Speech, and Signal Processing*, vol. 38, no. 12, pp. 2140–2150, 1990.
- [42] P. Stoica and A. Nehorai, “Performance study of conditional and unconditional direction-of-arrival estimation,” *IEEE Transactions on Acoustics, Speech, and Signal Processing*, vol. 38, no. 10, pp. 1783–1795, 1990.



**Hindawi**

Submit your manuscripts at  
[www.hindawi.com](http://www.hindawi.com)

